Journal of Alloys and Compounds 509 (2011) 9858–9864

Contents lists available at ScienceDirect

Journal of Alloys and Compounds

journal homepage: www.elsevier.com/locate/jallcom

# New application and electrochemical characterization of a nickel-doped mesoporous carbon for supercapacitors

S.R.P. Gnanakan[a], K. Karthikeyan[b], S. Amaresh[b], S.J. Cho[b], G.J. Park[c], Y.S. Lee[a,b,*]

[a] The Research Institute for Catalysis, Chonnam National University, Gwangju 500-757, Republic of Korea
[b] Faculty of Applied Chemical Engineering, Chonnam National University, Gwangju 500-757, Republic of Korea
[c] Department of Applied Chemistry, Saga University, 1 honjo, Saga 840-8502, Japan

ARTICLE INFO

*Article history:*
Received 18 March 2011
Accepted 15 July 2011
Available online 5 August 2011

*Keywords:*
Electric double layer capacitor
Activated carbon
Specific capacitance
Electrochemical properties
Organic electrolyte

ABSTRACT

A novel electrode of nickel-doped mesoporous carbon (NMC) is prepared from furfuryl alcohol and firstly developed for use in electrochemical capacitors. The electrochemical performance of NMC/AC capacitor is systematically investigated and characterized by BET and BJH methods for determining surface area and pore size distribution, respectively. This new NMC/AC shows a high specific capacitance, high energy and power density due to its large surface area and bulk conductivity. Its electrochemical characteristics are investigated through cyclic voltammetry (CV), electrochemical impedance spectroscopy and charge–discharge (C/D) tests. The NMC/AC has a specific capacitance of 144.3 $Fg^{-1}$, higher than that of a pure activated carbon (AC)-based EDLC (ca. 105 $Fg^{-1}$). It can be a promising candidate for a new energy storage material for supercapacitor.

Crown Copyright © 2011 Published by Elsevier B.V. All rights reserved.

## 1. Introduction

Electrochemical double layer capacitors (EDLCs) (ultracapacitors) are attractive energy storage devices suitable for a number of applications. The energy storage devices such as supercapacitors should have rapidly deliverable high energy densities [1]. The electrical energy ($E$) accumulated in such capacitors is given by: $E = (1/2)CU^2$, where ($C$) is the capacitance and ($U$) is the voltage. The high performance of the device depends on the optimization of these two parameters. The operating voltage is important in determining energy density, which depends on the stability window of the electrolyte. The operating voltage in aqueous electrolytes is 0.6–0.8 V, while in organic electrolytes it is 2.5–2.7 V. High energy storage and high capacitance have been observed in EDLCs with organic electrolytes. The structure of the double layer in organic electrolytes may be different from that in aqueous electrolytes.

EDLCs' wide applicability arises from their high specific surface area of carbon with highly attainable voltages in organic electrolytes. Chmiola et al. reported that micropores with diameters below 1 nm exhibit larger specific capacitances than those exhibited by materials with larger pores in non-aqueous electrolytes [2]. These results are against the commonly accepted idea that such micropores barely contribute to capacitance. The structure of the double layer in very small pores was proposed in their work to be different from that in relatively large pores. With this in mind, this work investigates the double layer capacitance of porous carbon in an organic electrolyte. The capacitance, $C$, depends on the electrode material and can arise through two mechanisms: (i) through purely electrostatic attractions between the charges of the electrodes and the electrolyte interface along electrical double layer (EDL), given by: $C = \varepsilon S/d$, where $S$ is the surface area, $\varepsilon$ is the dielectric constant and $d$ is the distance between the two electrodes; and (ii) through fast pseudo-faradaic charge transfer reactions in the device [3]. Although supercapacitors had delivered high energy densities but also exhibited very high equivalent series resistances; therefore they were only used in very low power memory backup applications. A variety of electrode materials have been studied for the development of supercapacitors with high energy densities and power capabilities. Supercapacitors employing metallic oxides [4–7] or conducting polymers [7–10] have been increasingly investigated for pseudo-faradaic charge transfer reactions, while carbon–carbon supercapacitors remain the most extensively studied and least expensive technology for industrial applications with high electrochemical stability.

Carbon materials have high surface area, good intra and inter particle conductivities in porous matrices. Furthermore, it has good electrolyte accessibilities with bulk electrical conductivities and minimal self-discharge rates. Recent research attention has focused on the application of nanostructured carbon as the electrode materials for energy storage applications. Chu and Braatz et al. studied many of the current supercapacitor systems [11]. The use of nanocarbon has the advantage of providing a larger

* Corresponding author at: The Research Institute for Catalysis, Chonnam National University, Gwangju 500-757, Republic of Korea. Tel.: +82 62 530 1904; fax: +82 62 530 1904.
*E-mail address:* leeys@chonnam.ac.kr (Y.S. Lee).

0925-8388/$ – see front matter. Crown Copyright © 2011 Published by Elsevier B.V. All rights reserved.
doi:10.1016/j.jallcom.2011.07.043

surface area through its nano or meso porosity. EDLCs use the strong ability of this material for charge accumulation (double layer) at the electrode/electrolyte interfaces. Frackowiak et al. [12] reported single-walled carbon nanotubes achieving a specific capacitance of 40 $Fg^{-1}$ and multi-walled carbon nanotubes reaching 80 $Fg^{-1}$. Park et al. [13] synthesized carbon nanotubes by plasma enhanced chemical vapor deposition and found them to show specific capacitances in the range of 33–82 $Fg^{-1}$ using non-aqueous aprotic organic solvent [$LiPF_6$ (EC/DEC)]. Diederich et al. [14] grew nanostructured carbon film at room temperature with a supersonic cluster beam; it demonstrated 75 $Fg^{-1}$. These are promising approaches in the search for high capacitance EDLCs. Porous carbon has been extensively studied because of its low cost and potential for high energy densities. Its main advantage is that it can be prepared with very high surface areas. Porous carbon with high surface area has a high fraction of micropores (pore size, <2 nm), but only a part of the surface is effectively utilized; most of the surface does not contribute to the double-layer capacitance and measured capacitance values are only ca. 20% of the theoretical maximum.

To improve these values, efforts have been made to develop mesoporous carbon for supercapacitors [15–17]. There are also various approaches to prepare mesoporous carbons using templating method [18–21]. It is well known that mesoporous silica such as MCM-41, SBA-15, MCM-48, etc. can be prepared using amphiphilic surfactant as structure directing agent with the formation of various micelle structures such as rod, cubic, lamellar etc. MCM-41 and SBA-15; can be made from the one-dimensional rod-like micelle structure using cetyltrimethylammonium cation and block copolymer surfactant, P123 as structure forming agents, respectively. On the other hand, MCM-48 can be obtained from the cubic micel structure and its structure is three-dimensionally connected Ia3d, facilitating mass transport through mesopores. Replication of MCM-48 with carbon can be performed in two different ways [22–24]. One is the simple impregnation of sucrose catalyzed acid and following carbonization at high temperature. The obtained carbon–silica composite is treated with HF or NaOH in order to remove the silica template, resulting in the mesoporous carbon. The other is the impregnation of furfuryl alcohol into the acid functionalized mesoporous silica. Thereby, the silica surface is coated with carbon after the carbonization. The removal of the silica template is resulted in the peculiar porous structure of mesoporous carbon. Thus, the obtained mesoporous carbon results in the improved electrochemical performance. The difference of carbon sources between sucrose and furfuryl alcohol was the degree of carbonization because furfuryl alcohol contained cyclic structure viable for graphitization with high C content compared to those of sucrose. The transition metals such as Fe, Co, Ni, etc. is known to accelerate the recrystallization of carbon into graphite as catalyst at high temperature [25,26]. It is also well known that the degree of graphitization depended on type of metal and Ni was employed as catalyst for recrystallization.

Thus, this paper firstly reports a novel electrode material, nickel-doped mesoporous carbon (NMC), a potential electrode for EDLCs. The NMC was characterized by physical and microstructural analyses. The specific capacitance, energy and power density were measured by fabricating electrochemical capacitors with NMC and AC electrodes that employed non-aqueous electrolyte. The results were compared with those from a pure AC-based conventional capacitor at the same time in this study.

## 2. Experimental

### 2.1. Materials and sample preparation

Transition metal catalyst was employed to prepare the nickel-doped mesoporous carbon with a crystalline pore wall from the carbonization of furfuryl alcohol inside Al-grafted MCM-48. The MCM-48 sample was prepared using cetyltrimethylammonium chloride (CTAC) and $C_{12}H_{25}O(C_2H_4O)_4H$ (Brij 30, Aldrich, USA) as a cationic–nonionic surfactant mixture [18]. An aqueous solution of sodium silicate with Na/Si = 0.5 was combined with aqueous solution of surfactant at room temperature and the resulting mixture was stirred vigorously for 1 h with a magnetic stirrer. The molar composition of the starting mixture was 5 $SiO_2$: 1.25 $Na_2O$: 0.85 CTAC: 0.15 Brij 30: 400 $H_2O$. This mixture was heated for 60 h at 373 K. After cooling to room temperature, the reaction mixture was neutralized drop by drop with an acetic acid that was equivalent to 60% of the Na content in the reaction mixture. The reaction mixture was heated again for 48 h at 373 K. The reaction mixture after cooling to room temperature was filtered, washed with doubly distilled water and then dried in oven at 373 K. The obtained as-synthesized MCM-48 was calcined in air flow to remove surfactant used as the template at 773 K for 6 h. Then, the obtained calcined sample was slurred in absolute ethanol solution containing a proper amount of $AlCl_3$. The obtained slurry was dried at 373 K, and calcined in air. Calcination temperature was increased linearly to 773 K over 6 h and maintained there for 5 h. The amount of the Si/Al ratio was controlled to 21.7.

The Al-grafted mesoporous silica was impregnated with nickel metal salts and dried in oven at 373 K for 12 h. $NiCl_2$ (>99%, Aldrich) was used as incorporated metal salts without further purification. The doped nickel contents into the Al-grafted mesoporous silica were 5 and 10 wt%, respectively, in this study. Furfuryl alcohol (FA) was soaked onto the sample containing metal complex, in which the FA to silica ratio in mass was controlled to 2.0. The polymerization of the furfuryl alcohol was performed by heating at 353 K for 2 h in a closed bottle and subsequently at 423 K for 8 h in an open container. The obtained polymerized furfuryl alcohol was heated at 1173 K for carbonization under a vacuum of 0.1 Pa. The carbonized carbon–silica composite was washed with 10 wt% HF twice to remove the silica template. The resulting nickel-doped mesoporous carbon was used as an electrode in an EDLC.

### 2.2. Electrodes preparation and test cell fabrication

Two electrodes with active materials of AC and NMC were prepared by mixing in ethanol the active material with ketzen black (KB) and teflonized acetylene black (TAB) at a weight ratio of 80:15:5. The mixture was formed into round homogenized film. The electrode films were cast on a 10 mm diameter stainless steel mesh and dried at 433 K for 4 h in a vacuum oven. All electrochemical measurements were performed with a two-electrode cell. The coin type cell (CR2032) was fabricated using the electrolyte 1 M lithium hexafluorophosphate ($LiPF_6$) in ethylene carbonate (EC) and dimethyl carbonate (DMC) (1:1 by v/v). A separator of micro-porous polypropylene (Celgard 3401) film and a glassy-fibrous filter (GB-100R) were soaked in electrolyte solution and then sandwiched between the two electrodes. The cell was fabricated in an argon-filled glove box.

### 2.3. Characterizations

The surface area and pore-size distribution of NMC were calculated from nitrogen adsorption isotherms (Micromeritics ASAP2010, USA) using the Brunauer, Emmett and Teller (BET) and Barrett, Joyner and Halenda (BJH) methods. Particle arrangements were studied by X-ray diffraction (XRD) patterns ($2\theta$ = 5–40°) using an X-ray diffractometer (Rigaku, Ultima III, Japan) equipped with a diffracted beam monochromater (Cu Kα radiation, λ = 1.5418 Å). The surface morphology of AC and the synthesized NMC were studied by field emission scanning electron microscopy (FE-SEM, S-4700, Hitachi, Japan) and transmission electron microscope (TEM, TechnaiF20, Philips, Netherlands), respectively. All electrochemical experiments were on two-electrode systems. The electrochemical performances of the supercapacitors were studied by cyclic voltammetry (CV) at scan rates of 1–100 $mVs^{-1}$ in the voltage range of 0–3.0 V. Electrochemical impedance spectroscopy (EIS) measurements were made in the range of 100 kHz to 10 mHz with an ac amplitude of 10 mV. Both CV and EIS were studied using an electrochemical analyzer (SP-150, Bio-Logic, France). Specific capacitance ($C_s$) was calculated by $C_S(F/g) = i/(s.r \times m)$; where $i$ is the average current, $s.r$ is the potential sweep rate and $m$ is the mass of electrode material. The capacitance and electrical series resistance (ESR) were determined by EIS. The charge/discharge measurements were carried out by galvanostatic cycling tests using a cycle life tester (WBCS 3000, Won-A-Tech, Korea) in the voltage limit 0–3.0 V at various current densities (1–5 mA $cm^{-2}$). The discharge specific capacitance ($C_{sp}$) was calculated by $C_{Sp}(F/g) = 4I/(dV/dt)m$; where $I$ is the current density (mA $cm^{-2}$), $t$ (s) is the discharge time with the discharge potential ($dV$) and $m$ (g) is the total weight of electrode material [27]. The power ($P_d$) and energy densities ($E_d$) were calculated by $P_d$ (W/kg) = $I$ (A) × $V$ ($v$)/$m$ (kg); and $E_d$ (Wh/kg) = $I$ (A) × $V$ ($v$) × $t$ (h)/$m$ (kg); where $I$ is the current density (mA $cm^{-2}$), $V$ is the discharge voltage excluding the IR drop occurring at the beginning of the discharge, $t$ is the discharge time and $m$ is the mass of active material in both electrodes.

## 3. Results and discussion

### 3.1. Physical characterizations

Fig. 1 shows the particle distributions and surface morphologies of AC and NMC by SEM and TEM analyses. The images show

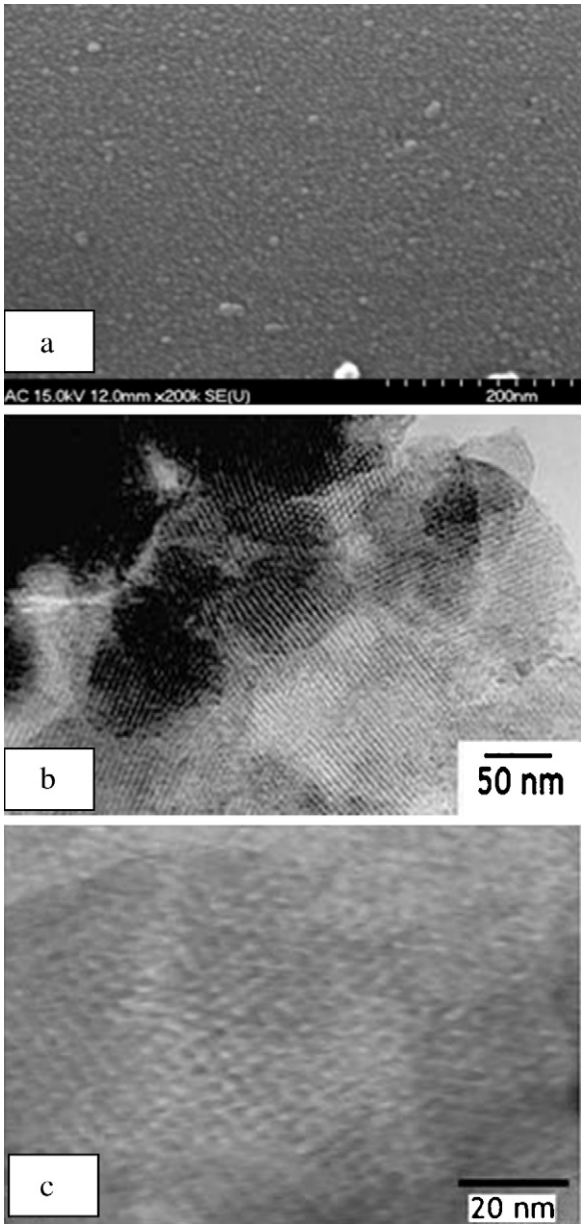


**Fig. 1.** SEM images of (a) activated carbon and (b) TEM image of NMC, and (c) magnification of (b).

that the AC particles were densely packed while the NMC particles were mesoporous. Fig. 1(b and c) clearly shows the TEM images of mesoporous carbon NMC network with uniform distribution, which can facilitate a higher surface area for better specific capacitance in supercapacitor system. The inter-connected carbon network greatly contributes to the high electrical conductivity. The diameter of the NMC particles was calculated to be few hundred nm and their pore sizes ranged from 2 to 3 nm. It can be expected that these pores enhance the ionic conduction in the electrode.

Fig. 2(a) shows wide-angle XRD patterns of prepared NMC materials. In the low angle region, it was confirmed that two characteristic peaks at $2\theta = 0.9^\circ$ and $2.5^\circ$ due to mesopore formation [18]. The XRD pattern of the mesoporous carbon was the inverse image of the silica structure were due to the carbon replication. With the increase of Ni content up to 5% and 10%, the peak intensity was increased progressively, suggesting the formation of mixture phase such as $Ni^0$, $Ni_3C$ and graphite. Broad diffraction peaks typical of disordered structures were observed at $2\theta = 23^\circ$ related to

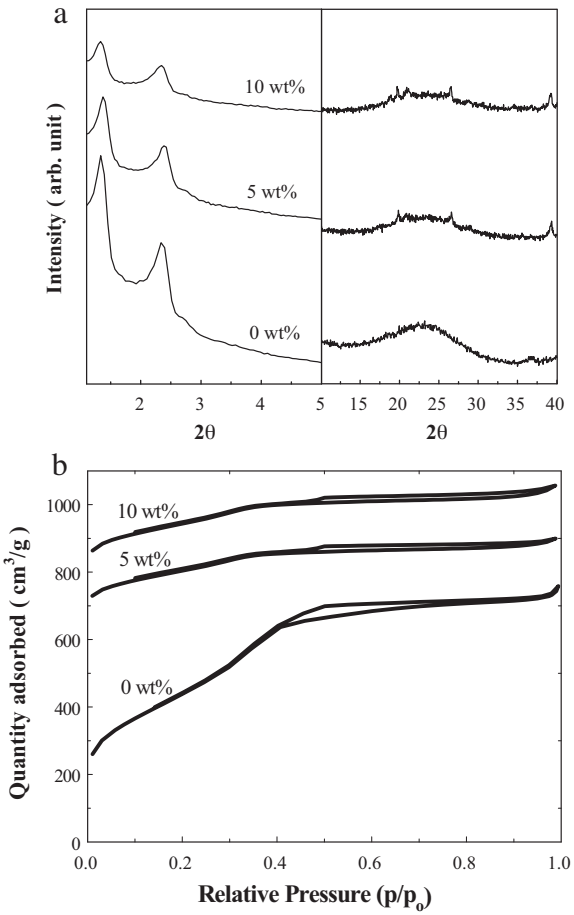


**Fig. 2.** (a) X-ray diffraction patterns of the porous carbons containing Ni metal after HF treatment as a function of metal content in the carbon–silica composite. The right and left panel shows the low and high angle region of XRD pattern, respectively; (b) $N_2$ BET adsorption–desorption isotherms of the porous carbons containing Ni metal at 77 K after HF treatment as a function of metal content in the carbon–silica composite.

the (002) reflection. Also, XRD peaks corresponding to the mixture of $Ni^0$, $Ni_3C$, and graphite were observed. Fig. 2(b) shows the $N_2$ adsorption–desorption isotherms at 77 K for NMC by BET measurements. The parent mesoporous carbon had the surface area of 1746 $m^2\,g^{-1}$ and the corresponding pore volume of 1.51 $ccg^{-1}$, respectively, as shown in Table 1. The surface area and pore volume were found to be $800 \pm 50\,m^2\,g^{-1}$ and $0.40 \pm 0.05\,ccg^{-1}$, respectively, with the incorporation of nickel. Therefore, the surface properties of the NMC were the same though the Ni content was changed. The $N_2$ adsorption–desorption isotherms for NMC show a modest hysteresis of nanopores at ca. $0.5P/P_0$ that was typical for mesoporous material.

The desorption branch of the nitrogen adsorption–desorption isotherm at 77 K was utilized to calculate the pore size as shown in Fig. 3. The parent mesoporous carbon showed the pore size of 3 nm, consistent with the previous reported value [18]. When nickel was incorporated, the pore size was decreased to 2.2 nm but it was not

**Table 1**
Summary of nitrogen adsorption–desorption isotherm at 77 K.

| Ni (wt%) | $S_{BET}$ ($m^2\,g^{-1}$) | $V_{pore}$[a] ($cm^3\,g^{-1}$) |
|---|---|---|
| 0 | 1746 | 1.51 |
| 5 | 730 | 0.38 |
| 10 | 854 | 0.43 |

[a] BJH desorption pore volume.

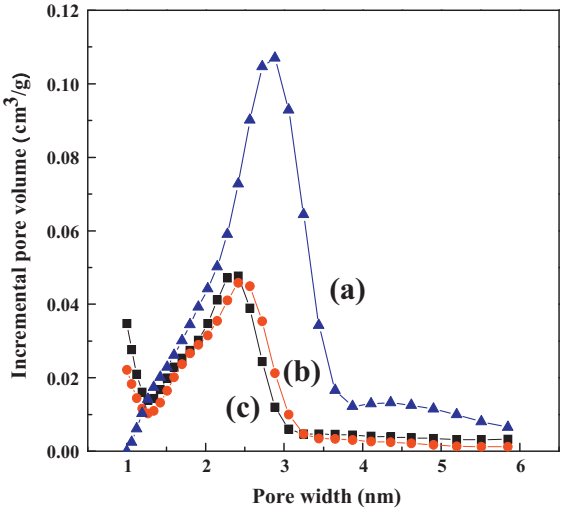


**Fig. 3.** BJH pore size distribution of the porous carbons containing Ni metal at 77 K after HF treatment as a function of Ni metal content (a) 0 wt%, (b) 5 wt% and (c) 10 wt%.

affected by the loading of nickel. It was of interesting to noteworthy that small pore fraction was increased slightly at 1 nm as shown in Fig. 3. In summary, the large surface area, pore volume and pore size distribution were maintained with the incorporation of nickel, which can be available for the electrochemical process.

### 3.2. Cyclic voltammetry

Fig. 4(a and b) shows cyclic voltammograms at various scan rates for the AC/AC and NMC/AC capacitors, respectively, where current was transferred to the capacitors based on the active material of the electrodes. For an ideal supercapacitor, the capacitance is independent of frequency, so that the charge stored is proportional to the voltage imposed by electrodes. Therefore, the current response will continue steadily at constant sweep rates ($mV\,s^{-1}$) during CV measurements. At the same scan rate, more ideal capacitive behavior was observed for NMC with a steeper current change at the switching potentials (0 and 3.0 V), resulting in a more rectangular *I–V* curve with no peaks attributed to electron transfer or redox reactions than AC/AC cell. The curves at different scan rates show no peaks, indicating that the electrode charged and discharged at a pseudo-constant rate over the complete voltammetric cycle. The slower changes at the switching potentials in the cyclic voltammograms of AC stem from the slower reorganization of the double layer owing to slower ionic motion in the mesopores. In addition, higher capacitances were obtained from NMC at all the applied scan rates, suggesting that the high surface area NMC made the electrode more accessible to electrolyte ions due to the improved wetability of the carbon and quicker charge propagation. The hydrophobization of NMC improved the affinity of the carbon surface to the non-polar organic solvents EC and DMC, and accordingly improved the electrodes' wetability. The CV shape of AC/AC cell at $100\,mV\,s^{-1}$ is smaller current area than $50\,mV\,s^{-1}$ scan rate, due to the stability of electrode material is limited to $50\,mV\,s^{-1}$.

Fig. 4(c) shows the specific capacitance of AC and NMC-based EDLCs as a function of scan rate. The specific capacitances were calculated to be $122\,Fg^{-1}$ and $93\,Fg^{-1}$ for the NMC and AC capacitors at $1\,mV\,s^{-1}$ sweep rate, respectively. These values are higher than those of carbon-based EDLCs in organic electrolytes [12–14]. Maximum specific capacitance was obtained at the scan rate of $1\,mV\,s^{-1}$. This is attributable to the high mesoporosity and high surface area of the NMC. Both particle size and porosity are important in determining the ability of the electrolyte to enter the electrode and to

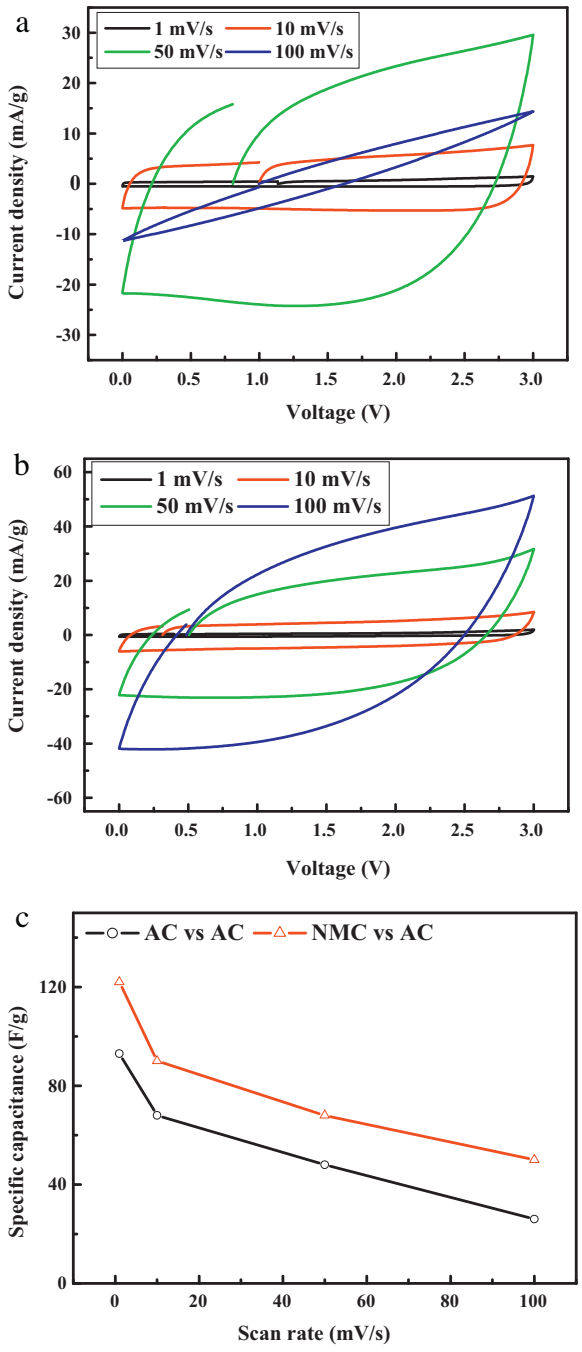


**Fig. 4.** Cyclic voltammograms at various scan rates ($1–100\,mV\,s^{-1}$) of the capacitors using (a) AC/AC, (b) NMC/AC, and (c) specific capacitance as a function of scan rate for both AC/AC and NMC/AC capacitors.

enable local ion transfer. However, specific capacitance decreases with increasing scan rate. The diffusing ions from the electrolyte can gain access to almost all available space in the electrode at low scan rates, leading to a complete insertion reaction. Increasing the scan rate reduces the effective interaction between ions and the electrodes and so increases the CV's deviation from rectangularity. The nanosized carbon provides shorter diffusion distances for ions penetrating the particles. High surface roughness and a porous structure permit the rapid insertion and extraction of electrolyte ions. Specific capacitances decreased to 72% and 60% for the AC and NMC-based EDLCs, respectively, when the scan rate increased from 1 to $100\,mV\,s^{-1}$.

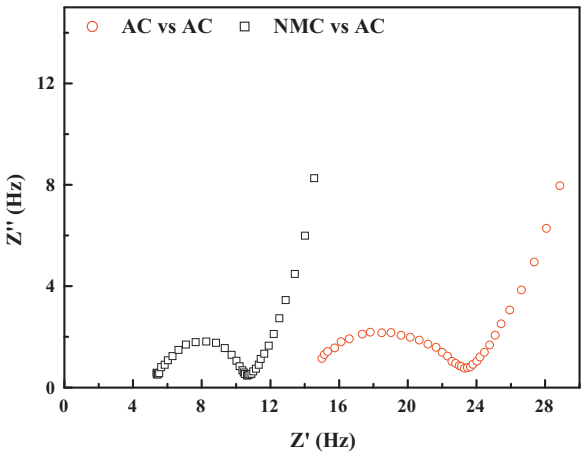


**Fig. 5.** Nyquist plots for AC and NMC-based capacitors in the frequency range of 100 kHz to 10 mHz.

### 3.3. Impedance studies

EIS calculates the resistances of the electrodes and electrolyte and evaluated their ionic and electronic conductivities as well as their specific capacitances. Fig. 5 shows Nyquist plots of the capacitors with AC and NMC electrodes. The semicircles observed at high frequency (100 kHz–400 Hz) represent a parallel combination of resistive and capacitive components. The electrolyte resistance ($R_s$) was calculated from the crossover point of the high frequency with the real part of the impedance. It was 5.3 and 14.9 Ω for the NMC and AC capacitors, respectively. Ionic or charge transfer resistances ($R_{ct}$) were estimated from the semicircle's diameter as 5.3 and 8.4 Ω for NMC and AC, respectively. The low values of $R_s$ and $R_{ct}$ for NMC are attributable to quicker mass transport within the mesopores and improved wetability; this indicates faster and higher electrolyte penetration of the electrodes. Another reason for the high conductivity is that the electrodes were partly de-doped in the tested potential range. These experimental results demonstrate that NMC may lead to faster electron transport in their inner pores and also form parallel double layers at their outer surfaces than that of AC. The charge-transfer complex formed by NMC endowed it with a higher degree of doping and a lower defect density, allowing it to facilitate charge transfer and lower its resistance compared with AC [28,29]. At low frequencies (<400 Hz), the impedance plots exhibit near vertical lines with respect to real part of impedance, indicating a limiting electrolyte diffusion process; this is a characteristic of pure capacitive behavior [30]. The capacitance increased at low frequencies due to the increased movement of ions that can decrease the capacitor's bulk resistance. The semicircle results from the parallel combination of resistance and capacitance and the linear region gives the Warburg impedance.

Further investigation of the performance of the capacitors' *RC* time constants (*R* and *C* are equivalent series resistance (ESR) and capacitance, respectively) was carried out. Larger *RC* time constants imply poorer rate capabilities. The capacitors' time constants were calculated from the frequency-dependent capacitance obtained in the low-frequency region according to the formula $C(f) = -i/2\pi fZ(f)$, where $i$, $f$ and $Z(f)$ are the imaginary unit, ac frequency and complex impedance at a frequency $f$, respectively. The time constant of the AC capacitor was 3 times that of the NMC capacitor, indicating that the NMC-based capacitor had an improved power capability. This is consistent with the CV tests.

### 3.4. Charge–discharge studies

The AC/AC and NMC/AC electrochemical capacitors were subjected to galvanostatic charge–discharge testing at various current

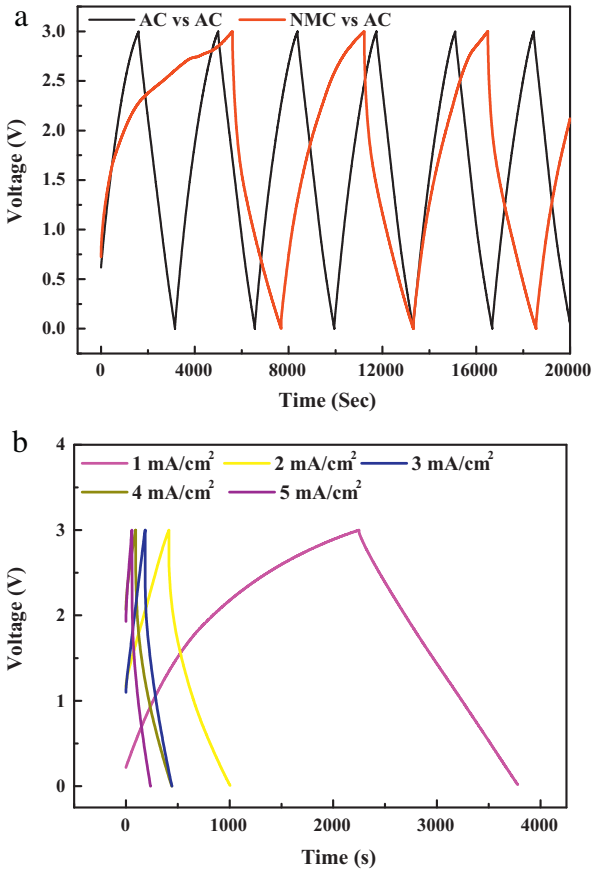


**Fig. 6.** (a) Charge–discharge curves of AC and NMC-based capacitors at 1 mA cm$^{-2}$ current density, (b) galvanostatic charge/discharge cycles at different current densities (1–5 mA cm$^{-2}$) of the NMC capacitor.

rates in the potential range of 0–3.0 V. The *V*–*t* curves show well-behaved multi-cycle triangular waves with minimal curvature for both the charge and discharge slopes at 1 mA cm$^{-2}$ (Fig. 6(a)). The charge and discharge curves are symmetrical over the whole potential range, implying that capacitance was mainly through pure electric double layer capacitance. $C_{sp}$ values were calculated as 105 Fg$^{-1}$ and 144.3 Fg$^{-1}$ for the AC/AC and NMC/AC EDLCs, respectively. The *C*/*D* curves of the NMC capacitor at various current densities are shown in Fig. 6(b). At low discharge currents, the response of the capacitor approached an ideal linear charge–voltage relationship. At high current rates, the total impedance of the cell gave rise to an initial drop of discharge voltage, which remained until constant capacitive performance was reached. A low discharge capacitance was associated with *iR* drop; *iR* drop is a direct measure of ESR, which influences the overall power performance of the capacitor. As the current density increased, the voltage rapidly decreased, consequently decreasing the discharge time and reducing $C_{sp}$. This is because at higher current densities only the outer layers of the active materials can contribute to charging and discharging, resulting in a decreased capacitance [31]. NMC showed a higher $C_{sp}$ than AC even at 5 mA cm$^{-2}$, mainly due to self-doping as well as its high surface area. The decrease in $C_{sp}$ were calculated as 55% and 45% for AC and NMC, respectively.

Fig. 7(a) shows specific capacitances and energy densities obtained at various discharge current rates for the AC/AC and NMC/AC capacitors. Specific capacitance continuously decreased with increasing discharge rate for both cells, attributable to the decreased sites for EDL formation. A slower decrease in capacitance with increasing discharge rate was observed for NMC than

**Table 2**
Discharge capacitance, energy and power densities with respect to discharge current density for AC/AC and NMC/AC capacitors.

| Discharge current density (mA cm$^{-2}$) | Discharge capacitance (Fg$^{-1}$) | | Energy density (Wh kg$^{-1}$) | | Power density (W kg$^{-1}$) | |
|---|---|---|---|---|---|---|
| | NMC/AC | AC/AC | NMC/AC | AC/AC | NMC/AC | AC/AC |
| 1 | 144.3 | 104.4 | 51.5 | 40.2 | 93.4 | 93 |
| 2 | 98.6 | 79.2 | 28.2 | 22.2 | 168.8 | 158 |
| 3 | 86.2 | 65.7 | 22.7 | 15.6 | 234.4 | 219 |
| 4 | 82.1 | 61 | 20.5 | 13.1 | 300.6 | 267.5 |
| 5 | 79.4 | 48 | 17.7 | 7.3 | 356.5 | 293.8 |

for AC, suggesting it had more rapid ion transport when under similar conditions. A similar tendency was also observed in the energy density. In comparison with specific capacitance, energy density noticeably decreased with increasing discharge rate due to additional effects of polarization resistance, which became the major source of energy loss at high discharge rates. The enhancement of capacitance and energy density in NMC is primarily attributed to the improvement of the electrode's wetability, resulting in more usable sites for EDL formation and lower internal resistance and consequently less energy loss. The stabilities of the electrodes were analysed through prolonged cycle-life testing at a constant discharge current of 1 mA cm$^{-2}$ over 1000 cycles (Fig. 7(b)). A small capacitance loss was observed after 100 cycles in both cells. After 1000 cycles, the $C_{sp}$ of NMC was maintained better than that of AC; it showed coulombic efficiency of >96%.

The measured specific capacitances, the power and energy densities of the AC/AC and NMC/AC capacitors at different discharge current densities are summarized in Table 2. Constant discharge at 5 mA cm$^{-2}$ yielded a power density of 356.5 W kg$^{-1}$, a reasonably high value. Higher power density is obviously achievable at higher current rates. However the energy density is low at high current densities, expected of supercapacitors employing non-aqueous electrolytes due to resistance and poor double layer formation. Such supercapacitors are typically suitable for pulse power applications, which involve high rate discharges.

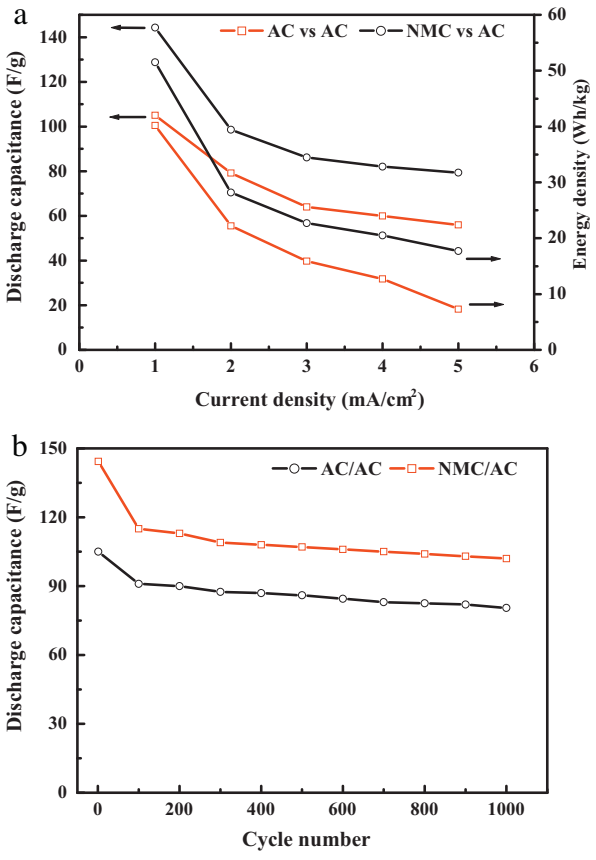


**Fig. 7.** (a) Discharge capacitance and energy density at various discharge current densities for AC/AC and NMC/AC capacitors. (b) Discharge capacitance with number of cycles for the AC/AC and NMC/AC capacitors at a current density of 1 mA cm$^{-2}$.

## 4. Conclusion

A new electrode material, nickel doped mesoporous carbon (NMC), was synthesized using furfuryl alcohol and firstly tested in an EDLC system. It was characterized by cyclic voltammetry, electrochemical impedance spectroscopy and galvanostatic charge/discharge tests. The improved electrochemical performance observed as a result of using NMC rather than conventional AC in the EDLC was largely due to the highly mesoporous nature of the material, its large surface area and excellent rate capability resulting from its interconnected carbon. Its specific capacitance was calculated to be 144.3 Fg$^{-1}$. Its energy and power densities were found to be 51.5 Wh kg$^{-1}$ and 93.2 W kg$^{-1}$, respectively. The stability of electrode was maintained even after 1000 cycles, inferred from coulombic efficiency and capacitance measurements. Nickel doped mesoporous carbon could be a promising material for high-power applications such as hybrid electric vehicles.

## Acknowledgements

This work was supported by Priority Research Centers Program through the National Research Foundation of Korea (NRF) funded by the Ministry of Education, Science and Technology (2010-0029626).

## References

[1] B.E. Conway, Electrochemical Supercapacitors, Kluwer Academic Plenum Publishers, New York, 1999.
[2] J. Chmiola, G. Yushin, Y. Gogotsi, P. Simon, P.L. Taberna, Science 313 (2006) 1760.
[3] E. Frackowiak, F. Beguin, Carbon 39 (2001) 937.
[4] J.P. Zheng, T.R. Jow, J. Electrochem. Soc. 142 (1995) L6.
[5] M. Toupin, T. Brousse, D. Belanger, Chem. Mater. 14 (2002) 3946.
[6] E. Raymundo-Pĩnero, V. Khomenko, E. Frackowiak, F. Beguin, J. Electrochem. Soc. 152 (2005) A229.
[7] Y. Zhang, H. Feng, X. Wu, L. Wang, A. Zhang, Int. J. Hydrogen Energy 34 (2009) 4889.
[8] M. Mastragostino, C. Arbizzani, F. Soavi, Solid State Ionics 148 (2002) 493.
[9] V. Khomenko, E. Frackowiak, F. Beguin, Electrochim. Acta 50 (2005) 2499.
[10] C. Peng, S. Zhang, D. Jewell, G.Z. Chen, Prog. Nat. Sci. 18 (2008) 777.
[11] A. Chu, P. Braatz, J. Power Sources 112 (2002) 236.
[12] E. Frackowiak, K. Jurewicz, S. Delpeux, F. Beguin, J. Power Sources 97 (2001) 822.
[13] D. Park, H.K. Young, K.L. Joung, Carbon 41 (2003) 1025.
[14] L. Diederich, E. Barborini, P. Piseri, J. Appl. Phys. Lett. 75 (1999) 2662.
[15] S. Yoon, J. Lee, T. Hyeon, S.M. Oh, J. Electrochem. Soc. 147 (2000) 2507.
[16] D. Lozano-Castelló, D.S. Shiraishi, H. Kurihara, A. Oya, Carbon 41 (2003) 1765.
[17] H. Zhou, S. Zhu, M. Hibino, I. Honma, J. Power Sources 122 (2003) 219.
[18] R. Ryoo, S.H. Joo, J.M. Kim, J. Phys. Chem. B 103 (1999) 7435.
[19] M. Kruk, M. Jaroniec, Y. Sakamoto, O. Terasaki, J. Phys. Chem. B 104 (2000) 292.
[20] D. Zhao, J. Feng, Q. Huo, N. Melosh, G.H. Fredrickson, Science 279 (1998) 548.
[21] J.-S. Lee, S.H. Joo, R. Ryoo, J. Am. Chem. Soc. 124 (2002) 1156.
[22] S.H. Joo, S.J. Choi, I. Oh, J. Kwak, Z. Liu, O. Terasaki, R. Ryoo, Nature 412 (2001) 169.

[23] R. Ryoo, S.H. Joo, M. Kruk, M. Jaroniec, Adv. Mater. 13 (2001) 677.
[24] T.-W. Kim, I.-S. Park, R. Ryoo, Angew. Chem. Int. Ed. 42 (2003) 4375.
[25] F.J. Maldonado-Hodar, C. Moreno-Castilla, J. Rivera-Utrilla, Langmuir 16 (2000) 4367.
[26] M. Inagaki, Y. Okada, V. Vignal, H. Komo, K. Oshida, Carbon 36 (1998) 1706.
[27] K. Karthikeyan, V. Aravindan, Y.S. Lee, et al., J. Alloys Compd. 504 (2010) 224.
[28] J. Zhang, L.B. Kong, B. Wang, Y.C. Luo, L. Kang, Synth. Met. 159 (2009) 260.
[29] Y.K. Zhou, B.L. He, W.J. Zhou, H.L. Li, J. Electrochem. Soc. 151 (2004) A1052.
[30] L.B. Kong, J. Zhang, J.J. An, Y.C. Luo, L. Kang, J. Mater. Sci. 43 (2008) 3664.
[31] M.A. Vorotyntsev, J.P. Badiali, G. Inzelt, J. Electroanal. Chem. 472 (1999) 7.